Rare Met. (2022) 41(1):106–114
https://doi.org/10.1007/s12598-021-01804-2

RARE METALS

ORIGINAL ARTICLE

Improvement of stability and solid-state battery performances of annealed $70Li_2S–30P_2S_5$ electrolytes by additives

Hao-Tian Ren, Zi-Qi Zhang, Jun-Zhao Zhang, Lin-Feng Peng, Zhen-Yuan He, Ming Yu, Chuang Yu*, Long Zhang*, Jia Xie, Shi-Jie Cheng

Received: 26 April 2021 / Revised: 3 June 2021 / Accepted: 7 June 2021 / Published online: 3 August 2021

Abstract The replacement of liquid electrolyte with solid electrolyte can significantly improve the safety and power/energy density of lithium batteries. $70Li_2S–30P_2S_5$ is one of the most promising solid electrolytes with high conductivity for solid–state batteries. In this work, the ionic conductivity and stability toward moisture and lithium metal of $70Li_2S–30P_2S_5$ were enhanced by introducing the different amounts of Li_2O additives. $65Li_2S–30P_2S_5–1\%Li_2O$ delivered the highest conductivity, while $65Li_2S–30P_2S_5–5\%Li_2O$ showed the best moisture stability and improved lithium compatibility. Solid-state batteries using $65Li_2S–30P_2S_5–5\%Li_2O$ electrolyte and high-voltage $LiNi_{0.6}Mn_{0.2}Co_{0.2}O_2$ cathode exhibited low initial discharge capacity (100 $mAh·g^{-1}$) and Coulombic efficiency (69%). Li_3InCl_6 electrolytes were introduced both in the cathode mixture to replace sulfide electrolyte and in the interface layer to improve the cathode compatibility for the solid-state batteries, showing enhanced discharge capacity (175 $mAh·g^{-1}$) and improved initial Coulombic efficiency (86%). Moreover, it also exhibited good performance at − 20 °C.

Keywords Solid electrolyte; $70Li_2S–30P_2S_5$; Stability; Additives; Solid-state batteries

Hao-Tian Ren, Zi-Qi Zhang and Jun-Zhao Zhang have contributed equally to this work.

Supplementary Information The online version contains supplementary material available at https://doi.org/10.1007/s12598-021-01804-2.

H.-T. Ren, J.-Z. Zhang, L.-F. Peng, Z.-Y. He, M. Yu, C. Yu*, J. Xie, S.-J. Cheng
State Key Laboratory of Advanced Electromagnetic Engineering and Technology, School of Electrical and Electronic Engineering, Huazhong University of Science and Technology, Wuhan 430074, China
e-mail: cyu2020@hust.edu.cn

Z.-Q. Zhang, L. Zhang*
Clean Nano Energy Center, State Key Laboratory of Metastable Materials Science and Technology, Yanshan University, Qinhuangdao 066004, China
e-mail: lzhang@ysu.edu.cn

L.-F. Peng
School of Physics, Huazhong University of Science and Technology, Wuhan 430074, China

C. Yu, J. Xie
Wuhan National High Magnetic Field Center and School of Physics, Huazhong University of Science and Technology, Wuhan 430074, China

1 Introduction

Solid-state batteries have attracted significant attentions due to their increased energy and power density and improved safety compared to the current lithium-ion batteries using liquid organic electrolytes [1–5]. Exploration of solid electrolytes with high ionic conductivity and high stability toward electrode materials can promote the development of solid-state batteries [6–8]. Intensive research efforts have been devoted to exploring and designing new kinds of solid electrolytes which can be applied in solid-state batteries [9]. Recently, sulfide solid electrolytes have exhibited great potential as one of the most promising candidates of solid electrolytes for solid-state batteries due to their high ionic conductivity and mechanical softness [10–15]. High ionic conductivity of solid electrolyte provides fast lithium-ion migration, and good mechanical softness property enables good interface

contact with electrode materials, both of which enable the possibility to fabricate solid-state batteries with excellent electrochemical performances [16, 17].

$Li_2S–P_2S_5$ system was reported as the most famous sulfide solid electrolytes with high ionic conductivity over 1×10^{-4} S·cm^{-1} at room temperature [18]. The ionic conductivities of $Li_2S–P_2S_5$ electrolytes are highly dependent on the ratio of Li_2S and P_2S_5 in the mixture of raw materials. The $Li_2S–P_2S_5$ amorphous glass solid electrolytes are usually synthesized via the high-energy mechanical milling process, and their ionic conductivity can be further enhanced after an annealing process [19]. Among those different compositions, the annealed $70Li_2S–30P_2S_5$ solid electrolyte showed a metastable phase with high ionic conductivity up to 1×10^{-3} S·cm^{-1} at room temperature, which can promote the development of solid-state batteries [20–24]. However, sulfide electrolytes suffer from the low chemical stability with moisture to generate H_2S, which increases the cost to fabricate solid-state batteries using $70Li_2S–30P_2S_5$ solid electrolytes. The low moisture stability was associated with S atoms in the structure, which can be easily reacted with H_2O to generate H_2S. Therefore, the replacement of S with O in the $70Li_2S–30P_2S_5$ solid electrolyte exhibited the possibility to enhance the moisture stability [25–31]. Moreover, sulfide electrolytes have redox reactive in contact with pristine high-voltage active material due to the great electrochemical potential differences [32, 33]. Surface modifications are the common route to avoid the direct contact between sulfide electrolytes and high-voltage cathode in the cathode mixture. However, homogenous coatings surround the whole particle are quite important. Another possible route to improve the compatibility of sulfide electrolytes toward high-voltage cathode is to replace the unstable sulfide electrolytes with high-stability electrolytes, such as lithium halide [34]. It has been reported that lithium halide solid electrolytes showed excellent compatibility with pristine high-voltage cathode materials [35, 36]. Therefore, the introduction of lithium halide additive in the cathode mixture and the interface layer to avoid the direct contact between sulfide electrolytes and pristine high-voltage cathode is a promising solution to enhance the electrode compatibility of sulfide electrolytes. Furthermore, solid-state batteries exhibited poor electrochemical performances at low temperature due to the decreased ionic conductivity and the slow kinetics of lithium-ions transport between the interface of electrode materials and solid electrolytes [37–41]. To fabricate solid-state batteries with acceptable performances and unravel the resistance evaluations during cycling at low temperature can promote the development of solid-state batteries.

In this work, we introduced Li_2O additives to partly replace Li_2S in $70Li_2S–30P_2S_5$ electrolyte to improve the moisture stability and lithium metal compatibility. The amounts of Li_2O additives were optimized to achieve high ionic conductivity and good stability toward moisture and lithium metal. The prepared solid electrolytes after modified by the Li_2O additives were combined with high-voltage cathode $LiNi_{0.6}Mn_{0.2}Co_{0.2}O_2$ and Li-In anode to fabricate solid-state batteries. Furthermore, Li_3InCl_6 electrolyte was introduced both in the cathode mixture to replace the sulfide electrolyte and in the interface of the above solid-state batteries to improve the electrochemical performance at different temperatures.

2 Experimental

2.1 Material synthesis

The solid electrolytes in this work were prepared through mechanical milling followed by a sintering process described in previous work [42–44]. Reagent-grade Li_2S (99.9%, Sigma-Aldrich), P_2S_5 (99%, Macklin), and Li_2O (99.9%, Sigma-Aldrich) powders were mixed with the required amount ratio using ZrO_2-coated stainless steel with ZrO_2 balls. The total weight ratio of ZrO_2 balls and the mixture of raw materials were fixed at 20/1. The total amount of the starting materials was 2.0 g for each jar. The mixture was first ball milled with a rotation speed of 500 r·min^{-1} for 12 h. The mixture obtained after the milling process was sealed in a quartz tube and annealed at 270 °C for 3 h to get the final solid electrolytes. Li_3InCl_6 was prepared by mechanical milling of the required amount of LiCl and $InCl_3$ with a rotation speed of 500 r·min^{-1} for 24 h followed by annealing the milled mixture at 260 °C for 5 h to obtain the final powder.

2.2 Material characterization

X-ray diffractometer (XRD) patterns of the annealed $(70–x)Li_2S–30P_2S_5–x\%Li_2O$ (x = 1, 2, 5, 10) solid electrolytes were collected using Cu Kα radiation from a SmartLab-SE Powder instrument over a 2θ range of 10°–70° to identify the phases. Morphology and energy-dispersive spectroscopy (EDS) mapping of the solid electrolytes were observed by scanning electron microscopy (SEM, Nova NanoSEM 450). Lithium-ion conductivities of the obtained solid electrolytes were characterized by pelletizing 100 mg target powder into a pellet (diameter of 10 mm) using stainless steel as the blocking electrodes. Alternating current (AC) impedance spectrum was performed with an impedance analyzer (Solartron, 1260) in the frequency range of 1 Hz to 10 MHz with an applied voltage of 0.02 V. Li/solid electrolyte/Li batteries were constructed to evaluate the lithium compatibility of $70Li_2S–30P_2S_5$ and $65Li_2S–30P_2S_5–5\%Li_2O$ as a function of the storage time.

The ionic conductivities of the Li_3InCl_6/65Li_2S–30P_2S_5–5%Li_2O bilayer solid electrolyte at different temperatures were characterized the same as the above description. The amounts of H_2S generated from the prepared solid electrolytes were measured by pelletizing 100 mg powder into a pellet with a diameter of 10 mm. The pressed pellet was transferred in a sealed plastic jar with a volume of 4 L, which was filled by moist air with a relative humidity of 60%–70%. The amount of H_2S was tested using an H_2S gas sensor as a function of time.

2.3 Solid-state battery fabrication and electrochemical measurement

For $LiNi_{0.6}Mn_{0.2}Co_{0.2}O_2$/65$Li_2S$–30$P_2S_5$–5%$Li_2O$/Li-In solid-state battery, 10 mg cathode mixture and 80 mg 65Li_2S–30P_2S_5–5%Li_2O electrolyte were pressed together by applying a pressure of 624 MPa, and then a piece of Li-In alloy was attached on the other side of the above bilayer pellet to form a triple-layer pellet using a pressure of 62.4 MPa. The cathode mixture for this battery was obtained by mixing the $LiNi_{0.6}Mn_{0.2}Co_{0.2}O_2$ with the 65Li_2S–30P_2S_5–5%Li_2O solid electrolyte with a weight ratio of 7/3. To fabricate the $LiNi_{0.6}Mn_{0.2}Co_{0.2}O_2$/$Li_3InCl_6$/65$Li_2S$–30$P_2S_5$–5%$Li_2O$/Li-In solid-state battery, 30 mg Li_3InCl_6 electrolyte and 50 mg 65Li_2S–30P_2S_5–5%Li_2O electrolyte were first pressed together with the same pressure and then combined the same amount of new cathode mixture, which consist of $LiNi_{0.6}Mn_{0.2}Co_{0.2}O_2$ and prepared Li_3InCl_6 electrolyte with the weight ratio of 7/3 to fabricate the final solid-state battery. The assembled solid-state batteries were charged/discharged at 0.1C between 2.4 and 3.7 V (vs. Li-In) at both room temperature and − 20 °C to evaluate the electrochemical performances. EIS before and after different cycles at different temperatures were measured in the frequency range of 1 Hz to 10 MHz with an applied voltage of 0.02 V.

3 Results and discussion

$Li_7P_3S_{11}$ solid electrolytes with different amounts of Li_2O additives were prepared by mechanical milling followed by an annealing process. XRD patterns of the prepared samples are shown in Fig. 1a. As illustrated, all the diffraction peaks of the obtained samples with different Li_2O additives were indexed to the pure phase of $Li_7P_3S_{11}$. Moreover, typical diffraction peaks due to $Li_7P_3S_{11}$ located at 18°, 24° and 30° once again confirmed that all those prepared electrolytes displayed similar structure as a function of the increasing Li_2O additives amount. The peak located at ~ 22° is attributed to the plastic film used for isolating moisture from the electrolytes. The ionic conductivities of $Li_7P_3S_{11}$ electrolytes with different amounts of Li_2O additives were characterized by temperature-dependent AC impedances. The lithium-ion conductivity of $Li_7P_3S_{11}$ was 1.0×10^{-3} S·cm^{-1}, increased to 1.2×10^{-3} S·cm^{-1} for 69Li_2S–30P_2S_5–1%Li_2O (1@7311), and then decreased to 8.4×10^{-4} S·cm^{-1} for 68Li_2S–30P_2S_5–2%Li_2O (2@7311), 9.9×10^{-4} S·cm^{-1} for 65Li_2S–30P_2S_5–5%Li_2O (5@7311), and 5.5×10^{-4} S·cm^{-1} for 60Li_2S–30P_2S_5–10%Li_2O (10@7311). The ionic conductivity of $Li_7P_3S_{11}$ first increased with the introduction of a small amount of Li_2O additive and then decreased with the introduction of a large amount of Li_2O additive. The ionic conductivities of those solid electrolytes with different amounts of Li_2O additive at different temperatures also confirmed this result, as shown in Figs. 1b, S1. 1@7311 electrolyte showed the highest ionic conductivity, and 10@7311 electrolyte displayed the lowest ionic conductivity among those solid electrolytes at different temperatures. As shown in Fig. 1c, the activation energy for conduction of those solid electrolytes first decreased with the introduction amount of Li_2O additives and then increased at a large introduction amount, such as 10%.

To validate the effect of introducing Li_2O on the air stability of $Li_7P_3S_{11}$ solid electrolyte, H_2S amounts generated from the prepared samples were investigated. Figure 1d displays the amounts of H_2S generated from the pelletized (70–x)Li_2S–30P_2S_5–$x$$Li_2O$ (x = 0, 1, 2, 5, 10) solid electrolytes. The addition of Li_2O additives plays a key point in the generation of H_2S gas from solid electrolytes after exposition to air at room temperature. H_2S gas generation rate and amount decreased after the introduction of Li_2O additives, indicating that introduction of Li_2O additives in $Li_7P_3S_{11}$ solid electrolyte is an effective modification route to improve the moisture stability. Owing to the higher stability of O than S in contact with moisture, partial replacement of S with O by the introduction of Li_2O additive during the synthesis can significantly enhance the moisture stability of sulfide solid electrolytes. The amount of H_2S gas increased as a function of the exposition time for all samples until reached the limit of the H_2S gas sensor. 5@7311 electrolyte showed the slowest H_2S gas generation rate among those solid electrolytes, suggesting the highest stability to moisture. Considering the acceptable lithium-ion conductivity and the best moisture stability of 5@7311 among those solid electrolytes, it was chosen as the solid electrolyte in this work. SEM images and EDS mapping images of the prepared 5@7311 solid electrolytes are performed and presented in Fig. 2. For comparison, SEM and EDS mapping images of $Li_7P_3S_{11}$ solid electrolyte are shown in Figure S2a–c. The electrolyte showed particles with diameter of larger than 10 μm and homogenous distribution of P, S and O. Previous research showed that the introduction of O can improve the stability

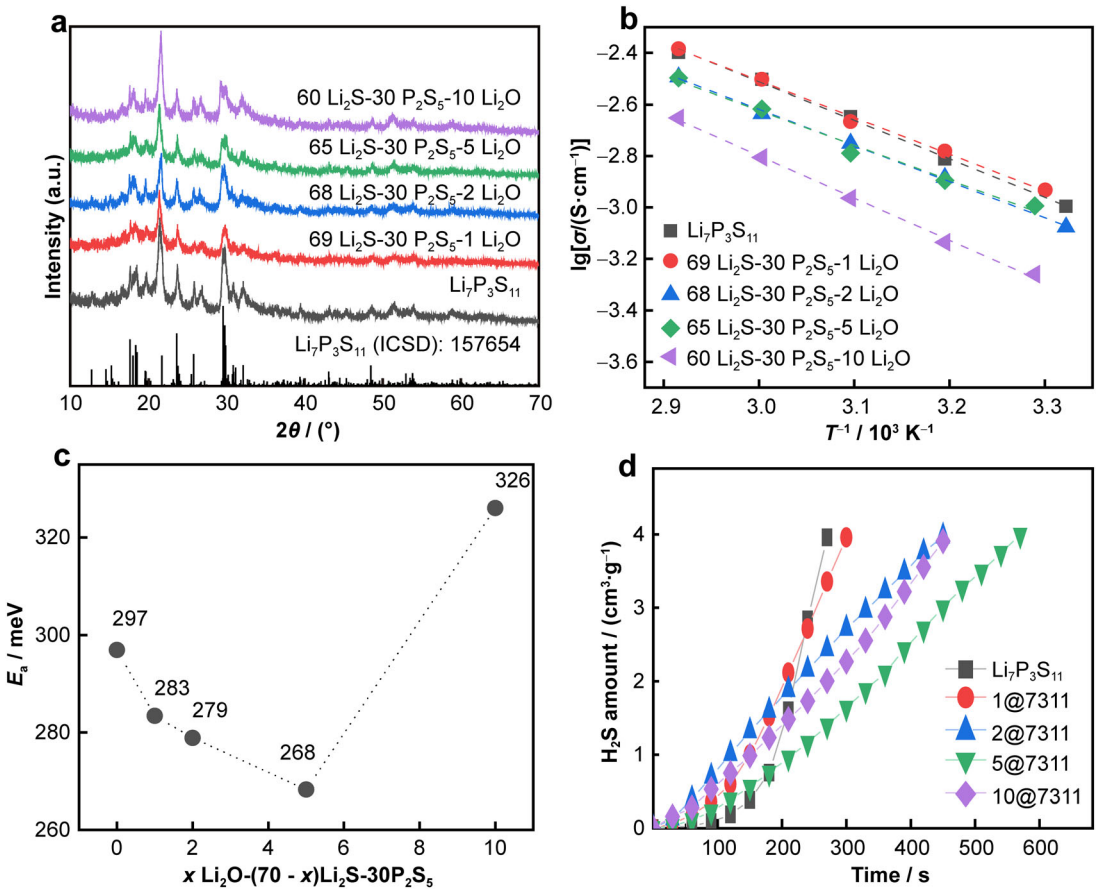

Fig. 1 **a** XRD patterns of $Li_7P_3S_{11}$ solid electrolytes with different amounts of Li_2O additives; **b** Arrhenius plots of corresponding prepared solid electrolytes; **c** changes of activation energy of solid electrolytes as a function of amount of Li_2O additives; **d** H_2S amount generated from pelletized $Li_7P_3S_{11}$ solid electrolytes with different amounts of Li_2O additives after exposition to air at room temperature for different storage durations

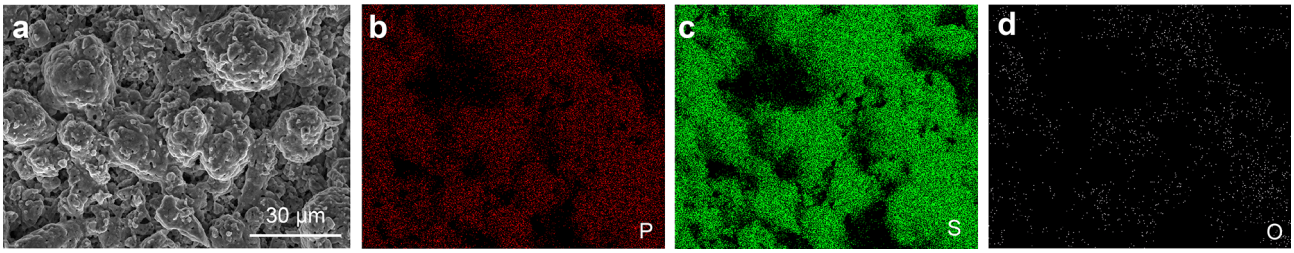

Fig. 2 **a** SEM image and **b–d** corresponding EDS mappings of prepared 5@7311 solid electrolyte

of sulfide electrolyte toward lithium metal. To verify the lithium compatibility of the electrolyte before and after adding the Li_2O additives, Li/5@7311/Li and Li/$Li_7P_3S_{11}$/Li batteries were constructed. As shown in Fig. 3a, b, the resistance of Li/ $Li_7P_3S_{11}$/Li battery increased as a function of the storage time with an extra resistance due to the chemical instability between lithium metal and $Li_7P_3S_{11}$ electrolyte. In contrast, the resistance showed slight changes with storage time increasing for the Li/5@7311/Li battery, suggesting a higher lithium metal compatibility than that of the bare $70Li_2S–30P_2S_5$ electrolyte. This also can be confirmed by the change of interfacial resistances for the assembled two batteries as a function of storage time, as illustrated in Fig. 3c. It has been reported that the chemical and electrochemical stability against lithium metal of Li_6PS_5Br electrolyte was enhanced with O doping [45]. The above results suggested that lithium metal compatibility and moisture stability of $Li_7P_3S_{11}$ electrolyte can be enhanced by the introduction of the Li_2O additives. To elucidate the inner mechanism of the improved compatibility between Li metal and $Li_7P_3S_{11}$ electrolyte, the XPS P 2p and S 2p detail spectra of $Li_7P_3S_{11}$ and 5@7311 were

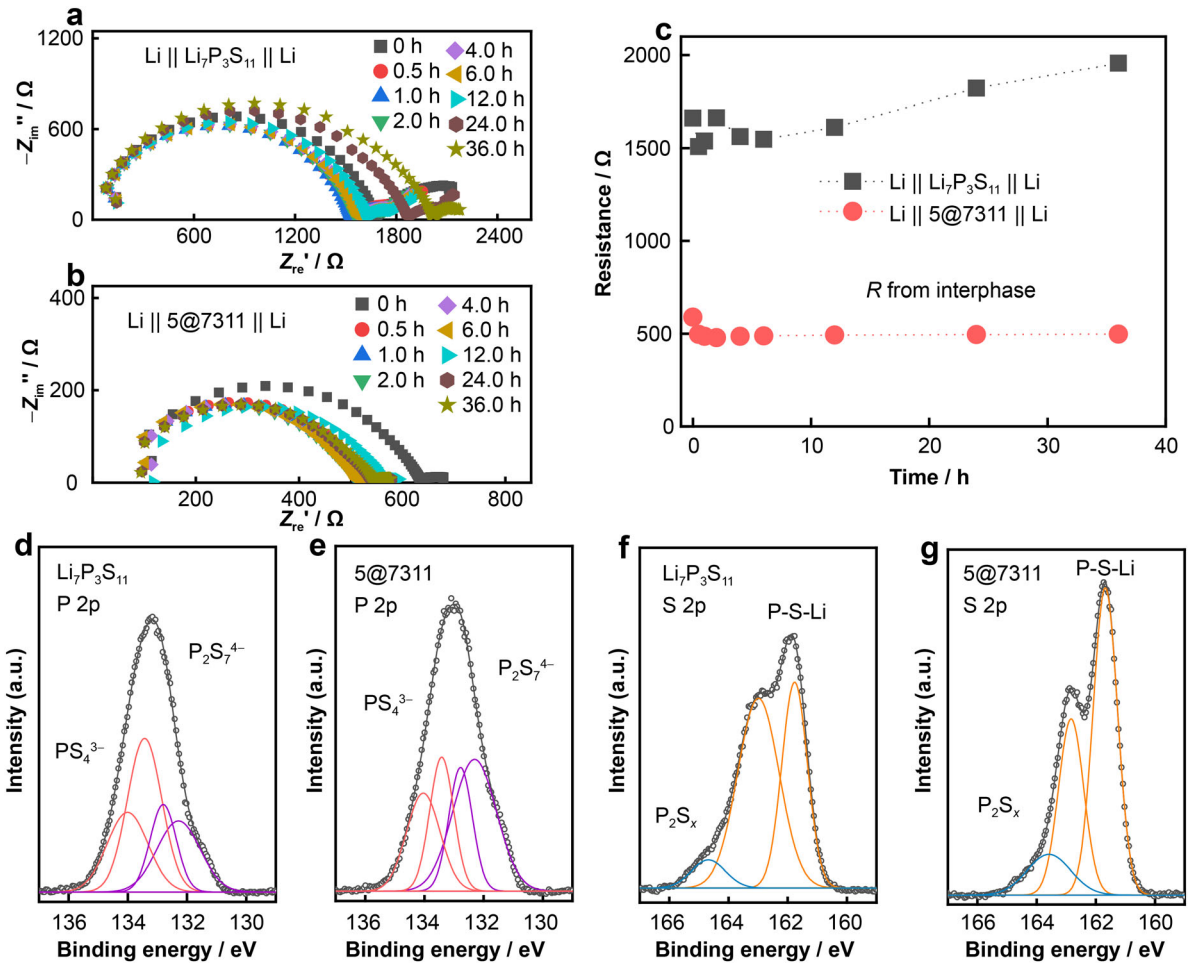

Fig. 3 Complex impedance spectra of **a** Li/$Li_7P_3S_{11}$/Li and **b** Li/5@7311/Li at different storage time at room temperature; **c** resistance variations as a function of storage durations; **d** XPS, **e** P 2p and **f**, **g** S 2p detail spectra of $Li_7P_3S_{11}$ and 5@7311 electrolytes

carried out. The ratio of PS_4^{3-} and $P_2S_7^{4-}$ groups was enhanced after introducing Li_2O in terms of P 2p results, as illustrated in Fig. 3d, e. Additionally, the S 2p result of 5@7311 showed impaired P_2S_x peak (Fig. 3f, g), which is consistent with the P 2p result. Therefore, the ameliorative Li metal compatibility of $Li_7P_3S_{11}$ electrolyte could be attributed to the reduced P–S–P bonding.

All solid-state batteries based on $Li_7P_3S_{11}$ and 5@7311 solid electrolytes in combination with the coated $LiNi_{0.6}Mn_{0.2}Co_{0.2}O_2$ and Li-In alloy were constructed and charged/discharged at 0.1C between 2.4 and 3.7 V (vs. Li-In) at room temperature. As shown in Fig. 4a, the $LiNi_{0.6}Mn_{0.2}Co_{0.2}O_2$/$Li_7P_3S_{11}$/In-Li battery delivered an initial charge capacity of 88 mAh·g^{-1} and discharge capacity of 54 mAh·g^{-1} with a low Coulombic efficiency of 61%. The $LiNi_{0.6}Mn_{0.2}Co_{0.2}O_2$/5@7311/In-Li delivered an initial charge capacity of 144 mAh·g^{-1} and discharge capacity of 100 mAh·g^{-1} with an enhanced Coulombic efficiency of 69%, as shown in Fig. 4b. After 10 cycles, the former maintained a discharge capacity of 33 mAh·g^{-1} with a discharge capacity retention of 61%, while the latter maintained a discharge capacity of 92 mAh·g^{-1} with a discharge capacity retention of 92%, as illustrated in Fig. 4c, d. EIS spectra before and after 10 cycles of above batteries were compared, as shown in Fig. 4e, f. The half-circle in the low frequency of the spectrum for cycled battery represents the resistance from the electrode and the solid electrolyte interfaces. The $LiNi_{0.6}Mn_{0.2}Co_{0.2}O_2$/5@7311/In-Li battery showed lower resistance compared to the $LiNi_{0.6}Mn_{0.2}Co_{0.2}O_2$/$Li_7P_3S_{11}$/In-Li battery, suggesting the improved compatibility of $Li_7P_3S_{11}$ electrolyte by introducing O atoms. Whereas $Li_7P_3S_{11}$ and 5@7311 solid electrolyte can directly contact with the pristine high-voltage $LiNi_{0.6}Mn_{0.2}Co_{0.2}O_2$ because the coated-$LiNi_{0.6}Mn_{0.2}Co_{0.2}O_2$ applied here was not homogenously coated, yielding interface reaction. The redox activity of sulfide electrolyte in the cathode mixture will cause a side reaction between the active material and electrolyte, leading to the formation of side reaction products at the interface with high interfacial resistance. The poor charge/discharge capacities and low initial Coulombic efficiency for the assembled solid-state battery here were due to the

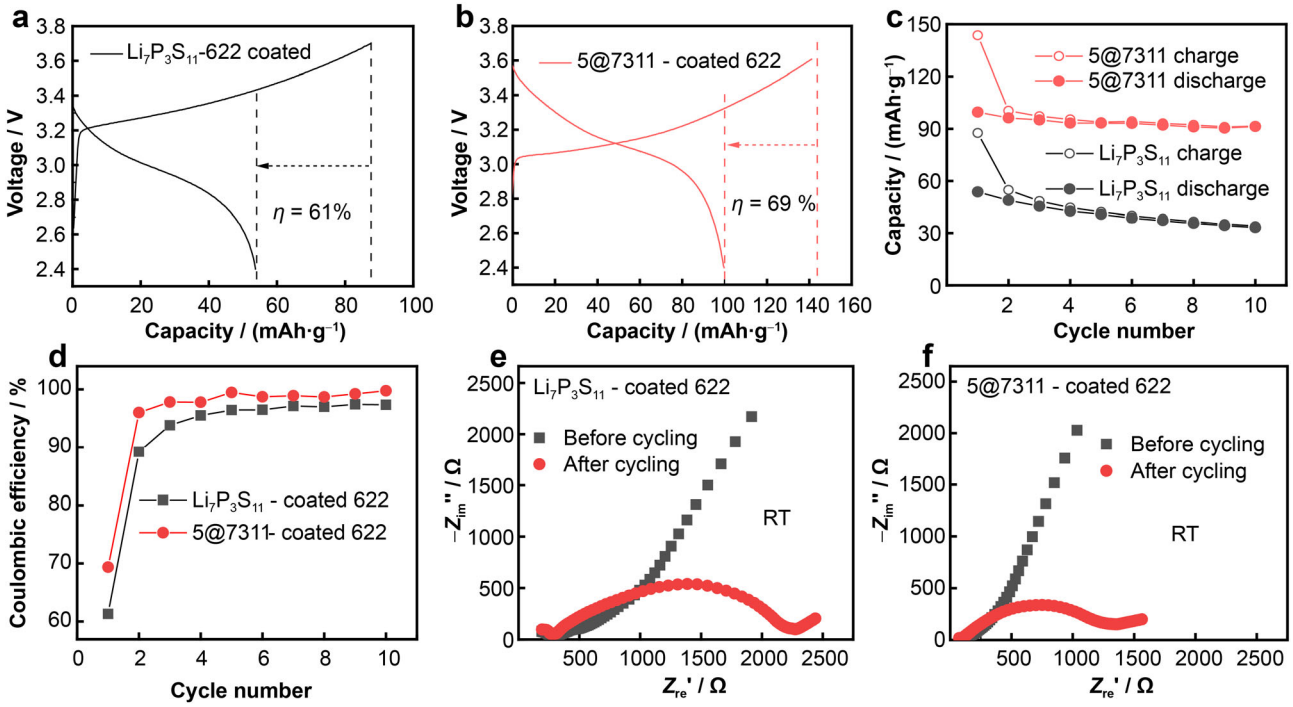

Fig. 4 Initial charge/discharge curves of **a** $LiNi_{0.6}Mn_{0.2}Co_{0.2}O_2/Li_7P_3S_{11}$/In-Li and **b** $LiNi_{0.6}Mn_{0.2}Co_{0.2}O_2$/5@7311/In-Li solid-state batteries cycled at 0.1C between 2.4 and 3.7 V at room temperature; **c** corresponding cycling performances and **d** Coulombic efficiency comparison; **e**, **f** EIS of above solid-state batteries before and after 10 cycles

incompatibility between the coated-$LiNi_{0.6}Mn_{0.2}Co_{0.2}O_2$ high-voltage cathode material and electrolyte.

Lithium halide solid electrolytes have been reported to exhibit excellent stability and compatibility with pristine high-voltage cathode material. To improve the stability of the cathode mixture, Li_3InCl_6 was synthesized and introduced to replace the high-voltage cathode instable 5@7311 electrolyte in the cathode mixture. Moreover, to separate the direct contact between the coated-$LiNi_{0.6}Mn_{0.2}$ $Co_{0.2}O_2$ and the prepared 5@7311 electrolyte layer, a thin layer of Li_3InCl_6 was introduced in the new designed solid-state battery. As shown in Figure S3a, a pure phase of Li_3InCl_6 (ICSD: 17638) was prepared by mechanical milling followed by an annealing route. The AC impedance spectra at different temperatures were performed using stainless steel as the blocking electrode, as shown in Figure S3b. The resistance of the prepared Li_3InCl_6 decreased as a function of the increasing testing temperature. It showed a room temperature ionic conductivity of 5.4×10^{-4} $S{\cdot}cm^{-1}$ with an activation energy of 0.40 eV for lithium-ion conduction, as illustrated in Figure S3c. SEM image and EDS mapping results exhibited large particle size with homogenous distribution of In and Cl (Figure S3d). To investigate the ionic conductivities of the 5@7311 and Li_3InCl_6 bilayer solid electrolytes, 30 mg Li_3InCl_6 and 50 mg 5@7311 electrolytes were pressed as a pellet using the same process with the same pressure. The resistance of this bilayer solid electrolytes increased with testing temperatures decreasing (Fig. 5a), delivering an ionic conductivity of 6.2×10^{-4} $S{\cdot}cm^{-1}$ at room temperature and 5.5×10^{-5} $S{\cdot}cm^{-1}$ at − 20 °C, respectively. The conductivities of 5@7311 and Li_3InCl_6 are 1.32×10^{-4} and 2.83×10^{-5} $S{\cdot}cm^{-1}$ at − 20 °C, respectively, as shown in Figure S4. As illustrated, the activation energy for lithium-ion conduction of the Li_3InCl_6/5@7311 bilayer solid electrolytes was 0.33 eV (Fig. 5b), which was lower than the activation energy of the Li_3InCl_6 electrolyte (0.40 eV) and higher than the activation of the 5@7311 electrolyte (0.27 eV).

To validate the effect of introducing Li_3InCl_6 electrolyte to replace sulfide electrolyte in the cathode mixture, $LiNi_{0.6}Mn_{0.2}Co_{0.2}O_2/Li_3InCl_6$/5@7311/Li-In solid-state battery was fabricated and charged/discharged with the same rate (0.1C) and voltage window (2.4–3.7 V (vs. Li-In)) at room temperature. As illustrated in Fig. 6a, it delivered an initial charge capacity of 204 $mAh{\cdot}g^{-1}$ and discharge capacity of 175 $mAh{\cdot}g^{-1}$ at room temperature with a Coulombic efficiency of 86%. After introducing the Li_3InCl_6 electrolyte additive in the cathode mixture and the interface layer between the cathode mixture and 5@7311 electrolyte, the new solid-state battery showed much higher charge/discharge capacities and Coulombic efficiency due to the improvement of compatibility between $LiNi_{0.6}Mn_{0.2}Co_{0.2}O_2$ active material and the 5@7311 electrolyte. This also confirms that Li_3InCl_6 electrolyte has

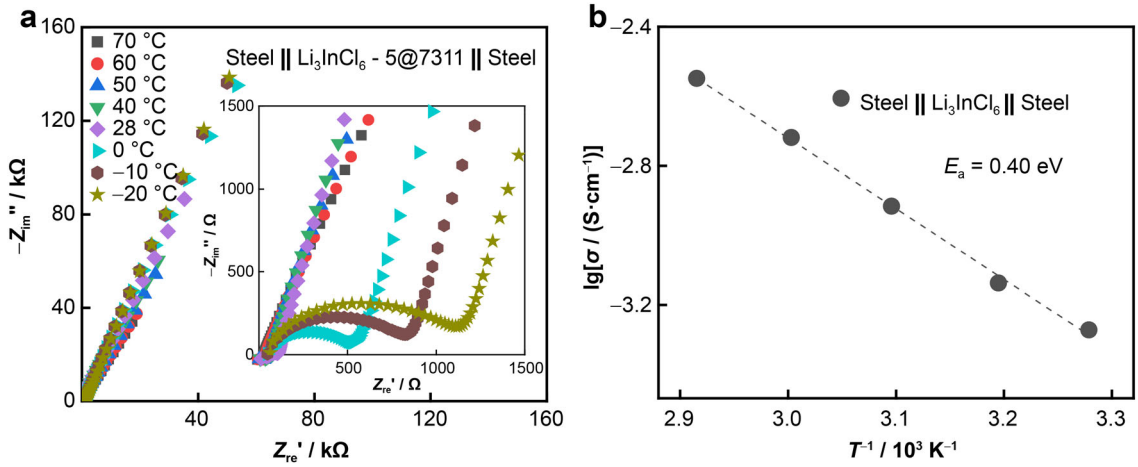

Fig. 5 **a** Complex impedance spectra of bilayer Li_3InCl_6 and 5@7311 solid electrolytes at different temperatures; **b** corresponding ionic conductivities at various temperatures

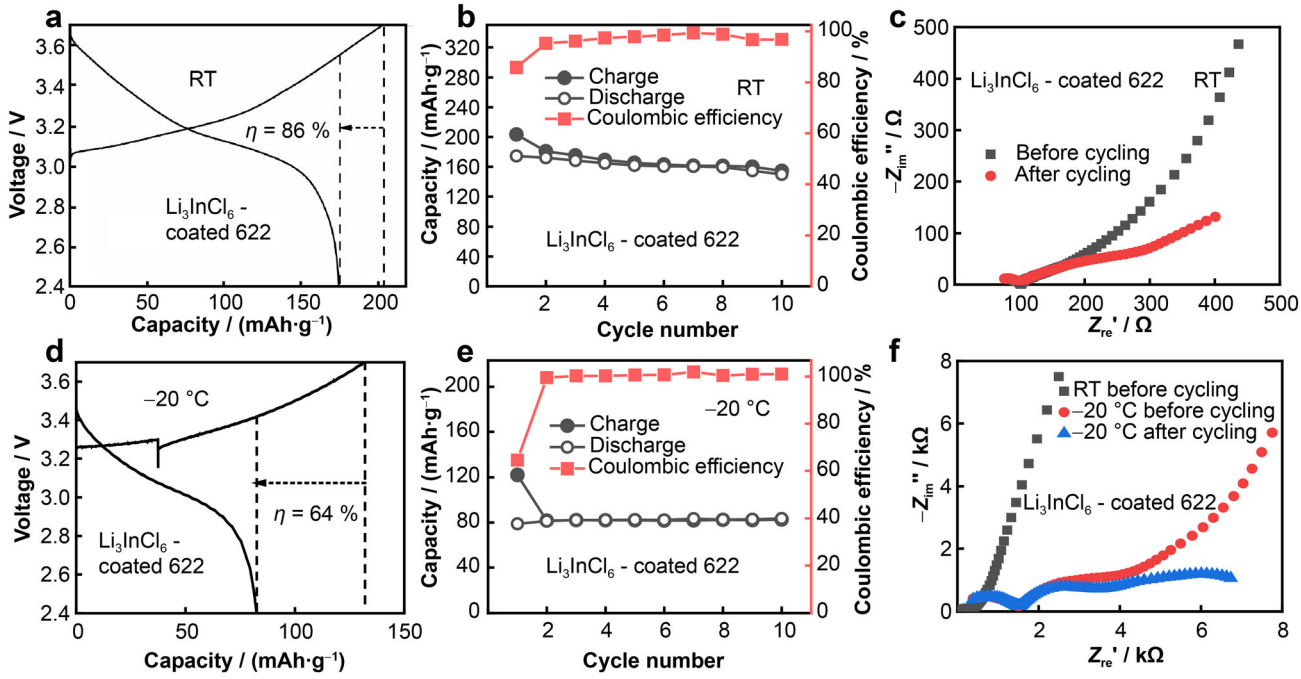

Fig. 6 **a** Initial charge/discharge curve and **b** corresponding cycling performances and Coulombic efficiency changes of $LiNi_{0.6}Mn_{0.2}Co_{0.2}O_2/Li_3InCl_6$/5@7311/In-Li solid-state battery using Li_3InCl_6 as solid electrolyte additive in cathode mixture cycled at 0.1C between 2.4 and 3.7 V (vs. Li-In) at room temperature; **c** corresponding EIS of solid-state battery before and after 10 cycles; **d** initial charge/discharge curve of above solid-state battery cycled at 0.1C between 2.4 and 3.7 V versus Li-In at − 20 °C; **e** corresponding cycling performances and Coulombic efficiency changes; **f** corresponding EIS of solid-state battery before and after 10 cycles

excellent stability with high-voltage cathode material. Further, 86% of the discharge capacity was retained after the 10th cycle (Fig. 6b). EIS before and after 10 cycles of the assembled solid-state battery showed that the 5@7311 electrolyte layer slightly changed, while the interfacial resistance from the $LiNi_{0.6}Mn_{0.2}Co_{0.2}O_2/Li_3InCl_6$ interface and the Li_3InCl_6/5@7311 was the major bottleneck for this battery (Fig. 6c). This also can be proved as the resistance change depicted in Figure S5. The resistance of Li_3InCl_6/5@7311/Li_3InCl_6 battery slightly increased as a function of the storage time, suggesting that the stability between Li_3InCl_6 and 5@7311 electrolyte still needs to be enhanced. For comparison, the battery of $LiNi_{0.6}Mn_{0.2}Co_{0.2}O_2/Li_3InCl_6$/Li-In with Li_3InCl_6 electrolyte as ionic conductor was assembled with the same rate (0.1C) and voltage window (2.4–3.7 V (vs. Li-In)) at room temperature (Figure S6). It delivered an initial charge capacity of 167 $mAh\cdot g^{-1}$ and discharge capacity of 132 $mAh\cdot g^{-1}$ at

room temperature with a Coulombic efficiency of 79%, and a discharge capacity retention rate of 47% after 10 cycles. It also demonstrated the design rationality of double-layer electrolyte structure. Finally, the low-temperature application of this solid-state battery was also investigated by charging/discharging the battery at 0.05C between 2.4 and 3.7 V under − 20 °C. The assembled $LiNi_{0.6}Mn_{0.2}Co_{0.2}O_2$/$Li_3InCl_6$/5@7311/Li-In battery exhibited much lower initial charge/discharge capacities, 122 and 79 $mAh·g^{-1}$, respectively, with a much lower Coulombic efficiency (64%), as shown in Fig. 6d. It showed stable cyclability in the subsequent 9 cycles at − 20 °C (Fig. 6e), delivered a discharge capacity of 80 $mAh·g^{-1}$ with almost undecayed capacity. The low charge/discharge capacities depicted here were associated with the low ionic conductivity of the Li_3InCl_6 electrolyte and the Li_3InCl_6/5@7311 solid electrolyte bilayer (5.5×10^{-5} $S·cm^{-1}$, − 20 °C) at low temperature. EIS results showed that two half circles belonged to the $LiNi_{0.6}Mn_{0.2}Co_{0.2}O_2$/$Li_3InCl_6$ interface and the Li_3InCl_6/5@7311 interface was observed when the temperature was lowered to − 20 °C, respectively. The resistance associated with the $LiNi_{0.6}Mn_{0.2}Co_{0.2}O_2$/$Li_3InCl_6$ interface was almost unchanged after 10 cycles, while the resistance attributed to the Li_3InCl_6/5@7311 interface slightly increased and the resistance due to the Li-In/5@7311 electrolyte was also observed (Fig. 6f).

4 Conclusion

In summary, the stability of $70Li_2S–30P_2S_5$ was improved by the introduction of Li_2O additives via mechanical milling followed by an annealing process. A small amount of Li_2O additives was introduced in the structure to enhance the ionic conductivity of $70Li_2S–30P_2S_5$ electrolyte, yielding the highest lithium-ion conductivity (1.2×10^{-3} $S·cm^{-1}$) at room temperature for $69Li_2S–30P_2S_5–1\%Li_2O$, while the ionic conductivities decreased with a higher amount of Li_2O additives. Moisture stability of the electrolyte was significantly enhanced by the replacement of S with O in the structure. The tailored $65Li_2S–30P_2S_5–5\%Li_2O$ electrolyte showed the highest moisture stability and improved compatibility toward lithium metal. $LiNi_{0.6}Mn_{0.2}Co_{0.2}O_2$/$65Li_2S–30P_2S_5–5\%Li_2O$/Li-In solid-state battery delivered enhanced charge/discharge capacities (144 and 100 $mAh·g^{-1}$) and initial Coulombic efficiency (69%) in comparison with $LiNi_{0.6}Mn_{0.2}Co_{0.2}O_2$/$Li_7P_3S_{11}$/Li–In battery (88 and 54 $mAh·g^{-1}$), which are still insufficient due to the redox reactivity of sulfide electrolyte in the cathode mixture toward high-voltage active material. Li_3InCl_6 electrolyte was successfully applied as the additive in the cathode mixture and the interface layer to avoid the direct contact of $LiNi_{0.6}Mn_{0.2}Co_{0.2}O_2$ and solid electrolyte. A solid-state battery with the structure of $LiNi_{0.6}Mn_{0.2}Co_{0.2}O_2$/$Li_3InCl_6$/$65Li_2S$-$30P_2S_5–5\%Li_2O$/Li-In was constructed and showed enhanced charge/discharge capacities (204 and 175 $mAh·g^{-1}$) and higher initial Coulombic efficiency (86%). The improvement of solid-state battery performance was due to the much lower interfacial resistance (∼ 200 Ω vs. 1000 Ω) after introducing Li_3InCl_6 additive. Furthermore, this solid-state battery even exhibited good electrochemical performance at an extremely low temperature (− 20 °C).

Acknowledgements This work was financially supported by the National Natural Science Foundation of China (Nos. 51821005, 21975087, U1966214 and 51902116), the Certificate of China Postdoctoral Science Foundation Grant (No. 2019M652634). We gratefully acknowledge the Analytical and Testing Center of HUST for allowing us to use its facilities.

Declaration

Conflict of interest The authors declare that they have no conflict of interest.

References

[1] Lee H, Oh P, Kim J, Cha H, Chae S, Lee S, Cho J. Advances and prospects of sulfide all-solid-state lithium batteries via one--to-one comparison with conventional liquid lithium ion batteries. Adv Mater. 2019;31(29):1900376.
[2] Randau S, Weber DA, Kötz O, Koerver R, Braun P, Weber A, Ivers-Tiffée E, Adermann T, Kulisch J, Zeier WG, Richter FH, Janek J. Benchmarking the performance of all-solid-state lithium batteries. Nat Energy. 2020;5(3):259.
[3] Lee YG, Fujiki S, Jung C, Suzuki N, Yashiro N, Omoda R, Ko DS, Shiratsuchi T, Sugimoto T, Ryu S, Ku JH, Watanabe T, Park Y, Aihara Y, Im D, Han IT. High-energy long-cycling all-solid-state lithium metal batteries enabled by silver–carbon composite anodes. Nat Energy. 2020;5(4):299.
[4] Tu Z, Choudhury S, Zachman MJ, Wei S, Zhang K, Kourkoutis LF, Archer LA. Fast ion transport at solid–solid interfaces in hybrid battery anodes. Nat Energy. 2018;3(4):310.
[5] Liu XZ, Ding L, Liu YZ. Room-temperature ionic conductivity of Ba, Y, Al co-doped $Li_7La_3Zr_2O_{12}$ solid electrolyte after sintering. Rare Met. 2021;40(8):2301.
[6] Xiao Y, Wang Y, Bo SH, Kim JC, Miara LJ, Ceder G. Understanding interface stability in solid-state batteries. Nat Rev Mater. 2019;5(2):105.
[7] Banerjee A, Wang X, Fang C, Wu EA, Meng YS. Interfaces and interphases in all-solid-state batteries with inorganic solid electrolytes. Chem Rev. 2020;120(14):6878.
[8] Xin Y, Gong JJ. Solid-state batteries: from fundamental interface characterization to realize sustainable promise. Rare Met. 2020;39(7):743.
[9] Jiang BX, Li YM, Wang ZM, Li ZK, Shen ZY. Electrical properties of Na-β″-Al_2O_3 solid electrolyte with Ti^{4+} doping. Chin J Rare Met. 2020;44(8):870.
[10] Wu J, Shen L, Zhang Z, Liu G, Wang Z, Zhou D, Wan H, Xu X, Yao X. All-solid-state lithium batteries with sulfide electrolytes and oxide cathodes. Electrochem Energy Rev. 2020;4(1):101.
[11] Zhang Q, Cao D, Ma Y, Natan A, Aurora P, Zhu H. Sulfide-based solid-state electrolytes: synthesis, stability, and

potential for all-solid-state batteries. Adv Mater. 2019;31(44):1901131.
[12] Yu C, Ganapathy S, Eck ER, Wang H, Basak S, Li Z, Wagemaker M. Accessing the bottleneck in all-solid state batteries, lithium-ion transport over the solid-electrolyte-electrode interface. Nat Commun. 2017;8(1):1086.
[13] Wu J, Shen L, Zhang Z, Liu G, Wang Z, Zhou D. All-solid-state lithium batteries with sulfide electrolytes and oxide cathodes. Electrochem Energy Rev. 2020;4(1):101.
[14] Zhang Z, Sun Y, Duan X, Peng L, Jia H, Zhang Y. Design and synthesis of room temperature stable Li-argyrodite superionic conductors via cation doping. J Mater Chem A. 2019;7(6):2717–22.
[15] Zhang Z, Zhang J, Jia H, Peng L, An T, Xie J. Enhancing ionic conductivity of solid electrolyte by lithium substitution in halogenated Li-argyrodite. J Power Sources. 2020;450(29):227601.
[16] Yu C, Ganapathy S, de Klerk NJ, Roslon I, van Eck ER, Kentgens AP, Wagemaker M. Unravelling Li-ion transport from picoseconds to seconds: bulk versus interfaces in an argyrodite Li_6PS_5Cl–Li_2S all-solid-state Li-ion battery. J Am Chem Soc. 2016;138(35):11192.
[17] Zhang Z, Zhang L, Liu Y, Yu C, Yan X, Xu B, Wang LM. Synthesis and characterization of argyrodite solid electrolytes for all-solid-state Li-ion batteries. J Alloys Compd. 2018;747(30):227.
[18] Minami K, Mizuno F, Hayashi A, Tatsumisago M. Lithium ion conductivity of the Li_2S–P_2S_5 glass-based electrolytes prepared by the melt quenching method. Solid State Ionics. 2007;178(11–12):837.
[19] Liu Z, Fu W, Payzant EA, Yu X, Wu Z, Dudney NJ, Kiggans J, Hong K, Rondinone AJ, Liang C. Anomalous high ionic conductivity of nanoporous β-Li_3PS_4. J Am Ceram Soc. 2013;135(3):975.
[20] Yamane H, Shibata M, Shimane Y, Junke T, Seino Y, Adams S, Minami K, Hayashi A, Tatsumisago M. Crystal structure of a superionic conductor, $Li_7P_3S_{11}$. Solid State Ionics. 2007;178(15–18):1163.
[21] Minami K, Hayashi A, Tatsumisago M. Crystallization process for superionic $Li_7P_3S_{11}$ glass-ceramic electrolytes. J Am Ceram Soc. 2011;94(6):1779.
[22] Hayashi A, Minami K, Ujiie S, Tatsumisago M. Preparation and ionic conductivity of $Li_7P_3S_{11-z}$ glass-ceramic electrolytes. J Non-Cryst Solids. 2010;356(44–49):2670.
[23] Seino Y, Ota T, Takada K, Hayashi A, Tatsumisago M. A sulphide lithium super ion conductor is superior to liquid ion conductors for use in rechargeable batteries. Energy Environ Sci. 2014;7(2):627.
[24] Prasada Rao R, Yuen JM, Adams S. Rechargeable lithium semi-flow battery using $Li_7P_3S_{11}$. Solid State Ionics. 2016. https://doi.org/10.1016/j.ssi.2016.01.015.
[25] Zhu Y, Mo Y. Materials design principles for air-stable lithium/sodium solid electrolytes. Angew Chem Int Ed Engl. 2020;59(40):17472.
[26] Liu H, Yang Z, Wang Q, Wang X, Shi X. Atomistic insights into the screening and role of oxygen in enhancing the Li^+ conductivity of $Li_7P_3S_{11}-O_x$ solid-state electrolytes. Phys Chem Chem Phys. 2019;21(48):26358.
[27] Guo Y, Guan H, Peng W, Li X, Ma Y, Song D, Zhang H, Li C, Zhang L. Enhancing the electrochemical performances of $Li_7P_3S_{11}$ electrolyte through P_2O_5 substitution for all-solid-state lithium battery. Solid State Ionics. 2020;358(15):115506.
[28] Ahmad N, Zhou L, Faheem M, Tufail MK, Yang L, Chen R, Zhou Y, Yang W. Enhanced air stability and high Li-ion conductivity of $Li_{6.988}P_{2.994}Nb_{0.2}S_{10.934}O_{0.6}$ glass-ceramic electrolyte for all-solid-state lithium-sulfur batteries. ACS Appl Mater Interfaces. 2020;12(19):21548.
[29] Zhao F, Alahakoon SH, Adair K, Zhang S, Xia W, Li W. An air-stable and Li-metal-compatible glass-ceramic electrolyte enabling high-performance all-solid-state Li metal batteries. Adv Mater. 2021;33(8):2006577.
[30] Liang J, Chen N, Li X, Li X, Adair KR, Li J. $Li_{10}Ge(P_{1-x}Sb_x)_2S_{12}$ lithium-ion conductors with enhanced atmospheric stability. Chem Mater. 2020;32(6):2664.
[31] Zhang Z, Zhang J, Sun Y, Jia H, Peng L, Zhang Y. $Li_{4-x}Sb_xSn_{1-x}S_4$ solid solutions for air-stable solid electrolytes. J Energy Chem. 2020. https://doi.org/10.1016/j.jechem.2019.05.015.
[32] Du M, Liao K, Lu Q, Shao Z. Recent advances in the interface engineering of solid-state Li-ion batteries with artificial buffer layers: challenges, materials, construction, and characterization. Energy Environ Sci. 2019;12(6):1780.
[33] Xu R, Han F, Ji X, Fan X, Tu J, Wang C. Interface engineering of sulfide electrolytes for all-solid-state lithium batteries. Nano Energy. 2018. https://doi.org/10.1016/j.nanoen.2018.09.061.
[34] Wang S, Bai Q, Nolan AM, Liu Y, Gong S, Sun Q, Mo Y. Lithium chlorides and bromides as promising solid-state chemistries for fast ion conductors with good electrochemical stability. Angew Chem Int Ed Engl. 2019;58(24):8039.
[35] Zhao X, Zhao-Karger Z, Fichtner M, Shen X. Halide-based materials and chemistry for rechargeable batteries. Angew Chem Int Ed Engl. 2020;59(15):5902.
[36] Li X, Liang J, Yang X, Adair KR, Wang C, Zhao F, Sun X. Progress and perspectives on halide lithium conductors for all-solid-state lithium batteries. Energy Environ Sci. 2020;13(5):1429.
[37] Park K-H, Kaup K, Assoud A, Zhang Q, Wu X, Nazar LF. High-voltage superionic halide solid electrolytes for all-solid--state Li-ion batteries. ACS Energy Lett. 2020;5(2):533.
[38] Riegger LM, Schlem R, Sann J, Zeier WG, Janek J. Lithium--metal anode instability of the superionic halide solid electrolytes and the implications for solid-state batteries. Angew Chem Int Ed Engl. 2021;60(12):6792.
[39] Yin J, Yao X, Peng G, Yang J, Huang Z, Liu D, Tao Y, Xu X. Influence of the Li–Ge–P–S based solid electrolytes on NCA electrochemical performances in all-solid-state lithium batteries. Solid State Ionics. 2015. https://doi.org/10.1016/j.ssi.2015.02.014.
[40] Qu H, Kafle J, Harris J, Zheng D, Koshina J, Boone D, Drake AM, Abegglen CJ, Qu D. Application of ac impedance as diagnostic tool—low temperature electrolyte for a Li-ion battery. Electrochim Acta. 2019;322(1):134755.
[41] Choi S, Jeon M, Kim BK, Sang BI, Kim H. Electrochemical behaviors of Li-argyrodite-based all-solid-state batteries under deep-freezing conditions. Chem Commun. 2018;54(100):14116.
[42] Seino Y, Nakagawa M, Senga M, Higuchi H, Takada K, Sasaki T. Analysis of the structure and degree of crystallisation of $70Li_2S$–$30P_2S_5$ glass ceramic. J Mater Chem A. 2015;3(6):2756.
[43] Busche MR, Weber DA, Schneider Y, Dietrich C, Wenzel S, Leichtweiss T, Schröder D, Zhang W, Weigand H, Walter D, Sedlmaier SJ, Houtarde D, Nazar LF, Janek J. In situ monitoring of fast Li-ion conductor $Li_7P_3S_{11}$ crystallization inside a hot--press setup. Chem Mater. 2016;28(17):6152.
[44] Mori K, Ichida T, Iwase K, Otomo T, Kohara S, Arai H, Uchimoto Y, Ogumi Z, Onodera Y, Fukunaga T. Visualization of conduction pathways in lithium superionic conductors: Li_2S-P_2S_5 glasses and $Li_7P_3S_{11}$ glass–ceramic. Chem Phys Lett. 2013;584(1):113.
[45] Zhang Z, Zhang L, Yan X, Wang H, Liu Y, Yu C, Cao X, van Eijck L, Wen B. All-in-one improvement toward Li_6PS_5Br--based solid electrolytes triggered by compositional tune. J Power Sources. 2019;410–411(15–31):162.